Eur. Phys. J. C (2005)
Digital Object Identifier (DOI) 10.1140/epjc/s2005-02331-9

THE EUROPEAN PHYSICAL JOURNAL C

In-medium effects on electromagnetic probes

C. Gale[a]

McGill University, Department of Physics, 3600 University Street, Montreal QC, Canada H3A 2T8

Received: 19 April 2005 /
Published online: 27 July 2005 –

Abstract. We discuss some of the aspects of the physics of relativistic nuclear collisions, in particular those having to do with the observation of electromagnetic radiation. We concentrate on what such measurements tell us about the local, in-medium properties of the environment from which they emerge. The contributions from different sources are considered: that from the partonic sector of QCD, and that from the confined hadronic phase. Specifically, we discuss the observation of real photons and of lepton pairs at the SPS and at RHIC, and make predictions for the LHC. The role of jets is discussed.

PACS. 25.75.-q, 12.38.Mh

1 Introduction

Electromagnetic radiation defines a privileged class of observables in the study of relativistic nuclear collisions. As real and virtual photons are only weakly coupled (in a parametrical sense) to the strongly interacting medium they are excellent probes of the local conditions at the time of their emission, because of the absence of final-state interactions. Of course, the physical interpretation of the information carried by such measurements also requires knowledge of the space-time evolution of the emitting medium. With those aspects in mind, we first recall the results of low-mass dilepton measurements at the SPS. We reiterate that those results are consistent with an interpretation in terms of vector spectral densities that are different from what they are in vacuum. We then show that those same spectral densities can be used to theoretically interpret the real photon spectrum, also measured at the SPS. Together with the intermediate invariant-mass regime, we conclude that the case for the observation of a new phase of QCD through electromagnetic measurements at SPS energies, even though suggestive, cannot be made convincingly. At still higher energies, photon production and jet quenching are considered consistently through jet–plasma interactions. We point out that this new source has even been seen at RHIC.

2 Low-mass lepton pairs

At SPS energies, the measurement of low-mass lepton pairs has first been made by the Helios/3 [1], and then by the CERES [2] collaborations. Those latter data represent the currently published state of the art. The theoretical interpretation of those measurements have been widely discussed elsewhere [3, 4]; however, it is worthwhile here to compare two approaches and to use this comparison to assess the control one has over the calculations. As a reminder, the rate of emission of dileptons is related to the retarded in-medium photon self-energy at finite temperature, $\Pi^{\rm R}_{\mu\nu}(E,q,T)$ [7]:

$$E_+E_-\frac{{\rm d}^6R_{\ell^+\ell^-}}{{\rm d}^3p_+{\rm d}^3p_-}=\frac{2e^2}{(2\pi)^6}\,\frac{n_{\rm B}(E,T)}{M^4}\,L^{\mu\nu}{\rm Im}\Pi^{\rm R}_{\mu\nu}(E,p,T), \tag{1}$$

where $n_{\rm B}(E,T)$ is a Bose–Einstein distribution function for energy E and temperature T, M is the invariant mass of the lepton pair ($M^2=(p_++p_-)^2$), and $L^{\mu\nu}=p_+^\mu p_-^\nu+p_-^\mu p_+^\nu-g^{\mu\nu}p_+\cdot p_-$. A similar expression is derived for real photons. Owing to the phenomenological success of vector meson dominance (VMD) [8], the current-field identity links the rate of electromagnetic emission directly to the in-medium vector spectral density. It is therefore clear that measurements involving real and/or virtual photons have the potential to reveal pristine features of the strongly interacting many-body system. The electromagnetic emissivity can be calculated in the hadronic sector by considering effective Lagrangians for the interacting fields, and then by evaluating the vector spectral density [3, 9]. Another approach consists of using the relationship between the self-energy and the forward scattering amplitude [10], and by modeling the latter by assuming that the dominant contributions are constituted of resonances coupled with a pomeron background [11]. There, the forward scattering amplitude is then fitted directly to experimental data. Those two approaches are of course related, but do constitute distinct avenues of investigation of a common theme. The in-medium vector spectral densities are computed, the

[a] e-mail: gale@physics.mcgill.ca

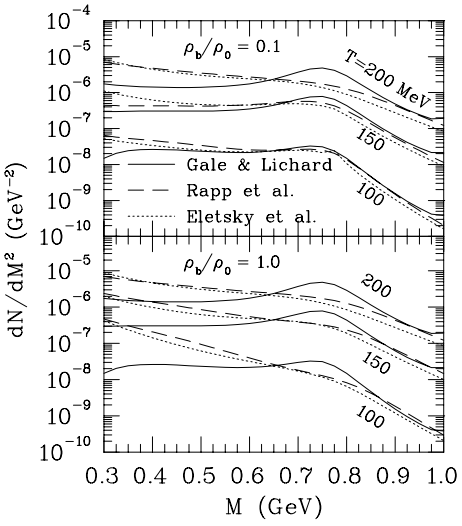

Fig. 1. A comparison [12] of the dilepton rates generated with the vector spectral densities obtained in the effective Lagrangian approach [3, 9], and through a direct experimental fit of the scattering amplitudes [11]. Also shown as a baseline is the result consisting of an incoherent sum of baryon-free channels [13]

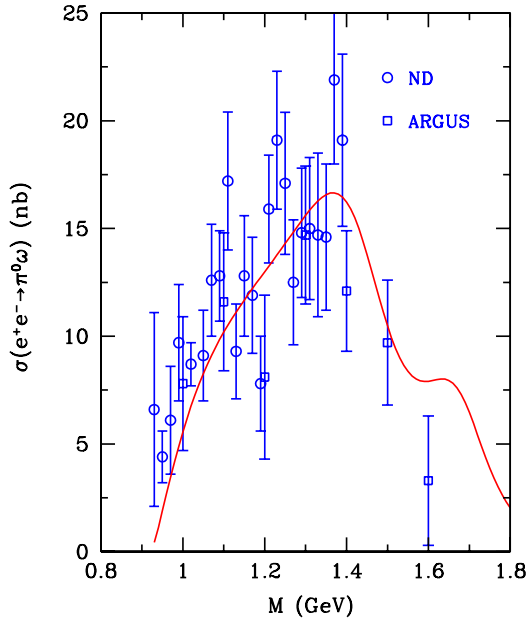

Fig. 2. The cross section for $e^+e^- \to \omega\pi^0$. The data are from the ND [17] and ARGUS [19] collaborations. The solid curve is generated from a model described in [17]

rates evaluated with (1), and the results are shown in Fig. 1. As a preamble, it is clear that the fitted scattering amplitudes can lose precision as the process moves further away from on-shellness, but the two approaches clearly yield very similar dilepton production rates over the temperature and density range shown here. This speaks for the robustness of the theoretical results and both those calculations contribute to the consensus of the need for modified in-medium spectrum densities to explain the low-mass dilepton data at the SPS [3–6]. The specific nature of the modification cannot be singled out by the current experimental data, but the importance of the enhancement at low energies is consistent with hadronic many-body calculations.

3 Intermediate-mass lepton pairs

At intermediate mass ($m_\phi < M < m_{J/\psi}$), the original estimates of the dilepton production rate to be appeared especially promising, as kinematical considerations combined with the original high temperature of the QCD plasma would highlight the intermediate invariant-mass region as the window of opportunity for the observation of plasma radiation [14, 15]. Now, whether one uses effective hadronic Lagrangian techniques or whether the self-energies are modeled directly from the available empirical data, as discussed previously, the same problem emerges. In both cases, the available parameters are fitted to measured physical properties which are softer than the scale defined by the intermediate lepton-pair invariant mass. In this case, the appearance of off-shell effects is a genuine concern. Indeed, different approaches that agree in the soft sector can yield widely different results in higher invariant-mass extrapolations [16]. Fortunately, constraints on the hadronic virtual photon-generating processes can be obtained through the wealth of data of the type $e^+e^- \to$ hadrons [17]. Those measurements cover precisely the same invariant-mass range as the one that concerns us here. They have been used, together with τ-decay data, to construct the axial vector and vector spectral densities that are related to the lepton-pair spectrum [18]. In addition, the intermediate-mass e^+e^- initial-state data have been analyzed specifically in a channel-by-channel fashion. An example is shown in Fig. 2. This information can then be used to derive the rates for hadrons $\to e^+e^-$. Following this procedure, the contributing channels for producing lepton pairs in the appropriate invariant-mass range are found to correspond to the initial states: $\pi\pi$, $\pi\rho$, $\pi\omega$, $\eta\rho$, $\rho\rho$, πa_1, $K\bar{K}$, $K\bar{K}^* + \text{c.c.}$. A detailed discussion is too long to be given here, but those channels are identified as the dominant ones, as their net lepton-pair contribution is found to saturate the spectral density analysis, at temperatures relevant for the experimental measurements at hand [20]. With some confidence in the microscopic rates, those can be integrated with an appropriate modeling of the space-time evolution of the colliding system.

Experimentally, an excess of intermediate invariant-mass dimuons over those from sources expected from p–A measurements has been confirmed by the Helios/3 [21] and NA50 collaborations [22]. We concentrate on the latter. Note (as in most experiments of this type) that it is important to properly account for the detector's finite acceptance, as well as for its resolution and efficiency. A numerical filter has been developed specifically for this purpose [23]. From the point of view of hard probes, this observed excess has generated a fair amount of interest. Indeed, this invariant-mass region is sensitive to the irreducible background constituted by correlated open charm semileptonic decay [24], and the excess can perhaps then be interpreted either as an increase in primordial $c\bar{c}$ abun-

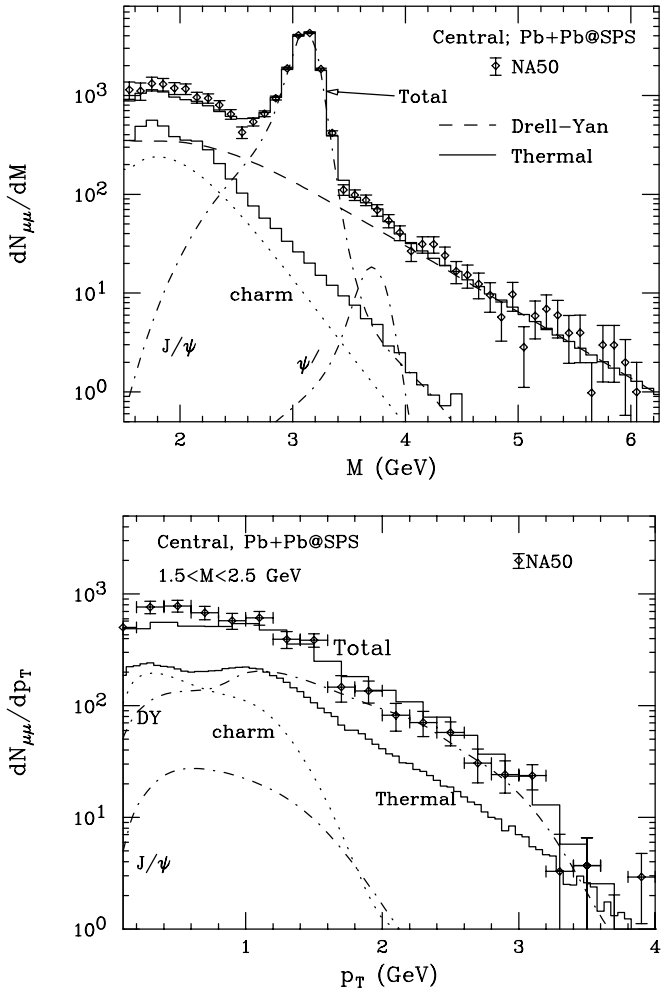

Fig. 3. The calculated dimuon invariant-mass and transverse momentum spectrum. The sources are Drell–Yan, correlated charm decay, direct charmonium decay, and thermal (quark–gluon plasma + hadron gas). The histogram represents the net contribution, after correcting for detector acceptance, resolution, and efficiency

dances, or as a kinematical broadening of the irreducible background generated by the rescattering of open charm mesons [25]. However, before more exotic explanations can be invoked, the contribution of thermal meson sources needs to be assessed quantitatively. A similar reasoning has been used in analyses of the Helios/3 [26] and NA50 [27] data.

Putting all of the elements described above together, we arrive at the spectra shown in Fig. 3. The parameters that enter this boost-invariant hydrodynamic calculation are the initial, critical and freeze-out temperatures. The set of those that is associated with Fig. 3 is 330, 180, 120 MeV. It is fair to say, however, that the initial temperature determination is somewhat dependent on the specific space-time modeling. However, a fairly robust conclusion still emerges: the intermediate-mass NA50 data do not demand a large radiation component from a plasma phase (it is about 20% here), nor does it require a large enhancement of the initial charm content. Even though the dynamical models differ in detail, this bottom line is shared by other studies of a similar nature [26–28]. The new high-precision data from NA60 [29] are eagerly awaited.

4 Low p_{T} photons

At SPS energies, real photon spectra have been measured by the WA98 collaboration [30]. Those data have been interpreted within several different approaches, such as hydrodynamic simulations [31], transport/cascade simulations [32], as well as using simple fireball models [33]. We describe here a recent calculation where the microscopic rates have been revisited, with emphasis put on basic hadronic phenomenology. We have already described the connection between the photon production rate and the in-medium vector spectral density. For self-energy topologies up to two loops, the imaginary part is readily shown to reduce to tree-level diagrams, in which case a kinetic theory approach proves to be convenient. In such a framework

$$E\frac{\mathrm{d}^3R}{\mathrm{d}^3q} = \int \frac{\mathrm{d}^3p_1}{(2\pi)^2 2E_1}\frac{\mathrm{d}^3p_2}{(2\pi)^2 2E_2}\frac{\mathrm{d}^3p_3}{(2\pi)^2 2E_3} \times(2\pi)^4\delta^{(4)}(p_1+p_2-p_3-q) \times|\mathcal{M}|^2\frac{f(E_1)f(E_2)[1\pm f(E_3)]}{2(2\pi)^3}. \quad (2)$$

Considering first the baryon-free sector, the elementary photon-producing reactions that involve light pseudoscalars, vectors, and axial vector mesons are evaluated in the massive Yang–Mills (MYM) formalism. This framework is capable of describing an adequate hadronic phenomenology with a limited set of adjustable parameters [34]. The vector and axial vector fields are treated as massive gauge fields of the chiral $\mathrm{U(3)_L \times U(3)_R}$ symmetry, and added to the non-linear σ model formulated in the exponential representation [35]. Note that this form of the interaction permits a coherent treatment of the strange and non-strange sectors of the theory, and thus does not suffer from phase ambiguities. Proceeding further, an expansion of the Lagrangian enables a systematic evaluation of all relevant processes. More specifically, all Born-level graphs with the appropriate crossing-symmetry partners were considered for reaction- and decay-type processes. An important consideration in applying effective hadronic models at moderate and high momentum transfers is the use of hadronic form factors. Those arise generally in effective models and are ubiquitous in hadronic physics. They are incorporated in the fits to hadronic properties, consistent with electromagnetic current conservation requirements [34]. Their effect at different temperatures may be judged from Fig. 4. An additional point worth mentioning in this context is that the ω vector meson is known to exhibit a large coupling to $\pi\rho$, and thus to $\pi\gamma$, owing to VMD. The on-shell radiative decay contribution is included in the early estimates of photon production [36], but its t-channel exchange in the reaction $\pi\rho \to \pi\gamma$ has not received much attention up to now. However, the usage of the hadronic form factors forces a re-calibration of the coupling constants. Because

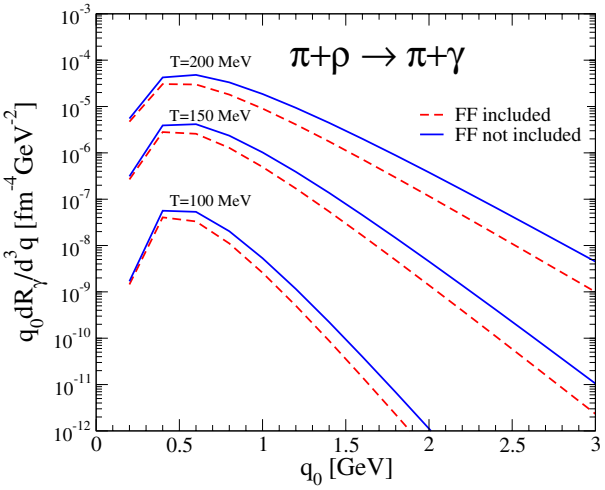

Fig. 4. Photon production rates at three different temperatures, showing the effect of form factors at hadronic vertices

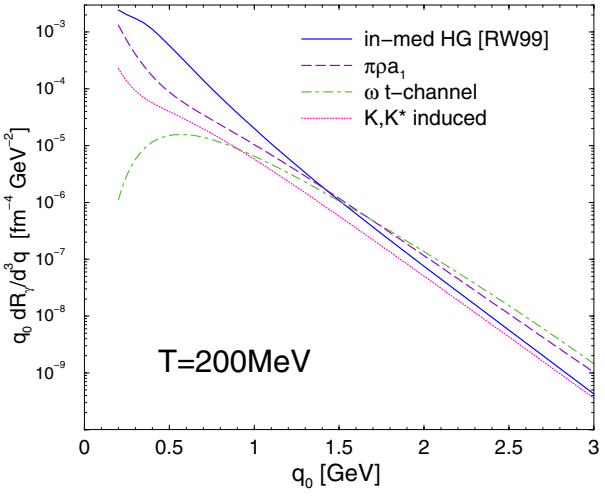

Fig. 5. Comparison of different sources for photon production in a hot and dense hadronic gas with $T = 200\,\mathrm{MeV}$, and baryon chemical potential $\mu_\mathrm{B} = 220\,\mathrm{MeV}$. The dashed and dotted curves represent the photon rates calculated in the MYM approach without the t-channel ω exchange. This latter contribution is shown by the dashed-dotted line. The full curve is the photon emissivity obtained with the vector spectral function approach including baryons

the $\omega\rho\pi$ vertex is constrained by the radiative decay width of the ω, and because this decay process involves an off-shell hadronic vertex (owing to VMD), the coupling is modified by the presence of the form factor. The size of this specific contribution can be assessed by considering the information in Fig. 5.

Since the emission of lepton pairs and that of real photons are linked to the same object, the in-medium photon self-energy, both should be calculable within the same formalism. This is what is done in the work we describe. Care has to be taken, as the leading-order contribution in both cases belong to different self-energy topologies. Moreover, the issues of double counting and coherence have to be considered. The a_1 s-channel graph is present in both the

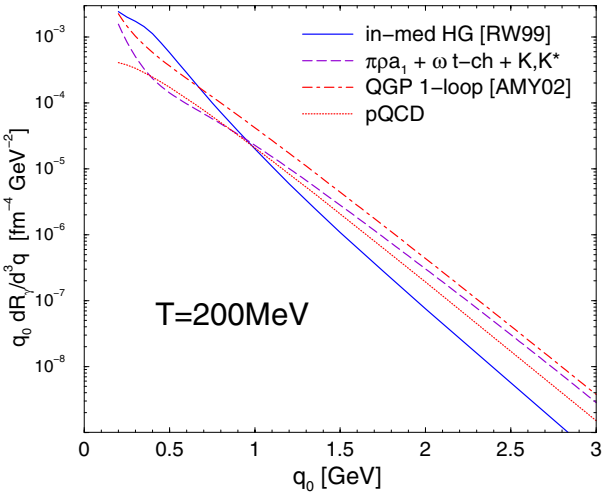

Fig. 6. Comparison of rates for photon production from a hot gas of partons. The solid line is from the many-body approach of [3], the dashed line represent the mesonic contributions, the dotted line is the HTL-corrected pQCD result, and the dashed-dotted line is the result that is complete at leading order in g_s

ρ spectral density and in the MYM framework. We remove it from the former, where it plays a minor role, whereas it induces non-negligible interference effects in the $\pi\rho a_1$ complex. If coherence is not important, the t-channel contributions may be evaluated separately. It was explicitly verified that this was the case for the ω exchange. The photon rate induced by bringing the vector spectral density to the photon point is shown in Fig. 5 by the solid line. It is instructive to compare the hadronic photon emission rates with those from a hot gas of partons at a similar temperature. This is done in Fig. 6. There, the spectral strength of the meson sources is compared with that in the baryon-rich sector, at a temperature of 200 MeV. Also shown is the hard-thermal-loop-corrected (HTL) result [36,56] (labeled pQCD), and the complete leading-order (in g_s) result for the photon emissivity of the quark–gluon plasma [37]. It would be useful to extract the required spectral density from lattice QCD calculations, but efforts there are only beginning [38].

Additional aspects need to be discussed before final yields can be derived. The emission rates again need to be integrated over the space-time history of the collision event. This is done here with a fireball model, which incorporates the main elements of hydrodynamic calculations. Soft photons are associated with sources which emit late in the space-time history of the reactions, and are thus sensitive to details of the flow profile. The details appear elsewhere [34,42], but using conservation laws one is able to extract the temperature and baryon chemical potential at any proper time, and to define a trajectory in the μ_B–T plane. The transition from the plasma to the hadronic gas phase is set at the chemical freeze-out locus experimentally extracted from hadron species ratios [39]. The hadronic gas is then evolved from chemical to thermal freeze-out by introducing the appropriate chemical potentials. The

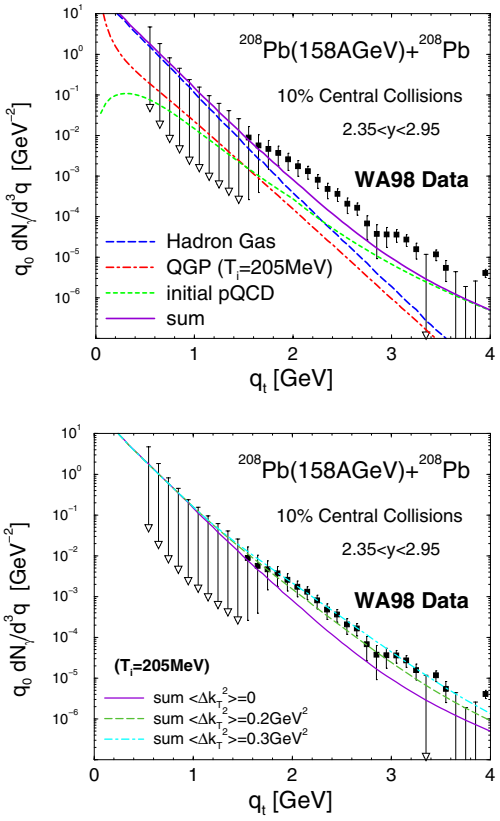

Fig. 7. Top panel: Thermal plus prompt photon spectra compared to data from WA98, for central Pb + Pb collisions at the SPS. Lower panel: the effect of the nuclear transverse momentum broadening on the measured photon spectrum. In analyses of p–A photon data, an adequate reproduction of the appropriate measurements emerges with a value of the broadening parameter $\langle \Delta k_{\mathrm{T}}^2 \rangle \simeq 0.1$–$0.2\,\mathrm{GeV}^2$

local photon momentum distributions are finally boosted to the lab frame, according to the time-dependent transverse expansion velocity that is eventually also found in the measured hadron transverse spectra. In addition, contributions to the direct photon spectra come from prompt photons emitted in primordial nucleon–nucleon collisions. An accurate theoretical description thereof at SPS energies is still a matter of debate [40]; therefore an empirical scaling relationship extracted from fits to data [41] is used. Finally, the transverse momentum broadening generated by the nuclear medium (Cronin effect) is estimated from analyses of the p–A data [34]. The result of considering all of the aspects discussed up to now, together with an adequate dynamical modeling of the nuclear collisions for the WA98 experiment appears on Fig. 7. The initial temperature used here is part of a global analysis of low- and intermediate-mass lepton-pair spectra [27, 42].

A partial summary is possible and appropriate here. As the primordial microscopic rates are very similar, it is increasingly clear that the differences in some of the intrinsic parameters of the various theoretical analyses, such as temperature, are related to differences in the space-time evolution. Nevertheless, the robust features here are that intermediate-mass lepton-pair spectra as well as low-mass dilepton and real photon spectra can be understood in terms of the hadronic degrees of freedom. Furthermore, low-mass dileptons and low p_{T} real photons are consistently calculated with the same spectral densities. The quark–gluon plasma component in all cases is not considerable enough to permit an unambiguous identification. For RHIC and the LHC, however, the situation is more promising [34], as we now discuss.

5 High p_{T} photons and jets

One of the most striking discoveries at RHIC has been that of the disappearance of the hadron–hadron correlation [43] and of the suppression of single-particle spectra in central nuclear collisions [44]. A compelling theoretical interpretation of those results is that of jet absorption in hot and dense partonic matter, signaling in effect the existence of a quark–gluon plasma. Several models of jet quenching through gluon bremsstrahlung have been elaborated [46–50]. Here, we shall report on results obtained using the approach developed by Arnold, Moore, and Yaffe (AMY) [51]. There, the initial hard gluon ($P_g(p, t = 0)$) and hard quark plus antiquark ($P_{q\bar{q}}(p, t = 0)$) probability distributions are evolved with time, as they traverse the medium. The joint equations for those quantities can be visualized as Fokker–Planck equations [52]. This technology permits one, given an initial jet profile calculated from zero-temperature QCD, to visualize its time evolution, as shown in Fig. 8. One may then investigate the effect of energy loss (and gain) on hadronic and electromagnetic observables. As mentioned previously, one variable that is often invoked in the context of jet quenching discussions is that associated with the suppression of single-particle momentum distributions. A quantitative measure of this suppression is shown in the so-called R_{AA} profile, where

$$R_{AA} = \frac{\mathrm{d}N_{AA}/\mathrm{d}y\mathrm{d}^2p_{\mathrm{T}}}{\langle N_{\mathrm{coll}}\rangle \mathrm{d}N_{pp}/\mathrm{d}y\mathrm{d}^2p_{\mathrm{T}}} \tag{3}$$

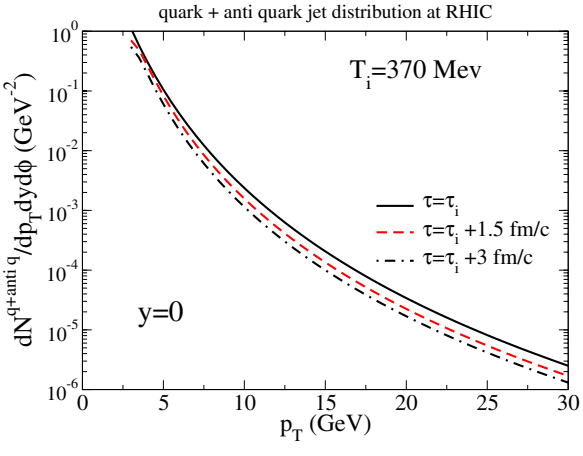

Fig. 8. The time-development of a quark (or antiquark) jet momentum profile, in an evolving parton medium. The initial distribution is obtained from a NLO calculation [53] that includes initial-state shadowing [54], for RHIC conditions

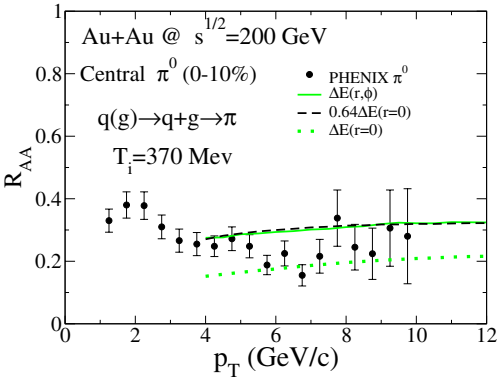

Fig. 9. R_{AA} for neutral pions measured by the PHENIX experimental collaboration. See text for details

is plotted as a function of transverse momentum. Clearly, if a nucleus–nucleus collisions is nothing more than a superposition of nucleon–nucleon collisions, then R_{AA} should be unity. The main points in the calculation of this quantity may be summarized here. First, in dense matter the parton distribution functions are different from what they are in proton–proton collisions [54]. Also, it is assumed that a jet fragments outside the strongly interacting medium, as suggested by formation time arguments, and that the fragmentation involves vacuum fragmentation functions. The effect of the medium is then to reduce the parton energy by an amount determined by the time evolution of the energy profile shown, for example, in Fig. 8. The jet starts in the QGP medium and evolves until it reaches the surface, or until the medium reaches the transition temperature, T_c. Note that we assumed that, at early times, the plasma could be modeled as following an isentropic 1D evolution, and that a first-order phase transition exists with a critical temperature of 160 MeV. Finally, it is important to point out that the spectrum calculated without energy loss is completely in agreement with measurements done in proton–proton collisions [52]. Note that since jets are emitted early in the collisions, the final profile shows only modest sensitivity to details of the time evolution [52]. For Au–Au central collisions at RHIC energy, we obtain the π^0 results shown in Fig. 9. We also assume a realistic spatial distribution for the jet initial location. Then, the neutral pion spectrum is obtained and shown by the full curve. If one makes the simplifying assumption that all jets originate from the center of the nucleus (which is not done in the rest of this work), one obtains the lower dashed curve. The third line shows that one is related to the other by a constant, up to a very good approximation. Within the formalism of AMY, the only explicit parameter in this calculation that is not common to other phenomenological studies of RHIC results (both hadronic and electromagnetic; see for example [34]) is the strong coupling constant, α_s. We use $\alpha_s = 0.3$.

If the physical conditions for jet quenching are realized, they do signal a jet–plasma interaction. By the same argument, this interaction can manifest itself through other probes, some of which may be electromagnetic. Previous estimates have shown that the conversion of a leading parton to a photon in the plasma was found to be an important source of real photons [55]. This means that a jet crossing the hot medium undergoes an annihilation ($q + \bar{q} \to g + \gamma$) or a Compton process ($g + q \to q + \gamma$) with a thermal parton. The contribution to the photon production rate in a finite-temperature parton medium for the leading topology is known to be [55, 56]

$$\frac{\mathrm{d}R}{\mathrm{d}y\mathrm{d}^2p_\mathrm{T}} = \sum_f \left(\frac{e_f}{e}\right) \frac{T^2\alpha\alpha_\mathrm{s}}{8\pi^2} \left[f_q(\boldsymbol{p}_\gamma) + f_{\bar{q}}(\boldsymbol{p}_\gamma)\right] \times \left[2\ln\left(\frac{4E_\gamma T}{m^2}\right) - C_\mathrm{ann} - C_\mathrm{Comp}\right], \quad (4)$$

where T is the temperature, $C_\mathrm{ann} = 1.916$, and $C_\mathrm{Comp} = 0.416$. In a hot QCD medium, the infrared singularity that appears in the limit of vanishing quark mass, $m \to 0$, gets screened by hard thermal loops: $m^2 = 4\pi\alpha_\mathrm{s}T^2/3$ [36, 56]. The incoming parton may now be the leading parton in a jet, and then strikes a thermal parton. However, the jet evolving in the QCD medium has lost energy and this is accounted for with the technology described earlier. We term this photon source "jet-thermal", in an obvious nomenclature. The net photon spectrum will also receive contributions from sources identified with primordial hard nucleon–nucleon collisions, with the jet fragmenting into a photon (and hadrons, after loosing energy), with the jet producing photons via bremsstrahlung interactions as it traverses the medium (and loses energy), and with photons produced through interactions of thermal plasma constituents [52]. The emissivity in those different channels is integrated over the space-time history, with initial conditions appropriate for RHIC and the LHC, and the result is shown in Fig. 11. Both at RHIC and LHC energies, it is satisfying to note that the original premise of this exercise still holds true: the jet–plasma photons are an important source, which in fact outshines others at $p_\mathrm{T} \sim 4\mathrm{GeV}/c$ for RHIC, and at $p_\mathrm{T} \sim 8\mathrm{GeV}/c$ for the LHC. At RHIC, real photon data already exist and there are much more to come. An early analysis concentrated on the ratio of the total number of photons to background photons:

$$\frac{\gamma_\mathrm{total}}{\gamma_\mathrm{background}} = \frac{\mathrm{d}^3N_\gamma^\mathrm{bck}/\mathrm{d}^2p_\mathrm{T}\mathrm{d}y + \sum \text{all other sources}}{\mathrm{d}^3N_\gamma^\mathrm{bck}/\mathrm{d}^2p_\mathrm{T}\mathrm{d}y}. \quad (5)$$

This quantity is plotted in Fig. 10, together with data from PHENIX [57], with and without the thermal contribution. The calculation including the thermal component is in good agreement with the data, except for a few points in the range $7 < p_\mathrm{T} < 9\,\mathrm{GeV}/c$. Without the thermal components the agreement worsens considerably. The small effect of varying the initial temperature is also seen on the same figure.

6 Summary

Soft electromagnetic spectra (low-mass dileptons and low p_T photons) receive an important contribution from hadronic sources. We have shown results where the emissivity has been derived from the same in-medium spectral

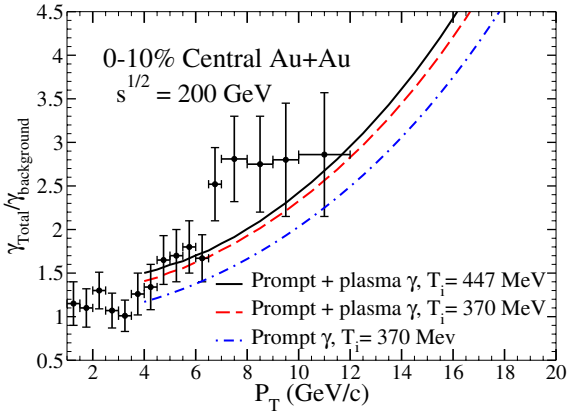

Fig. 10. The ration of all photons over the decay photons is shown, for Au–Au collisions at RHIC energies, with and without the thermal contribution. The effect of varying the initial temperature is also shown. The data are from the PHENIX collaboration [57]

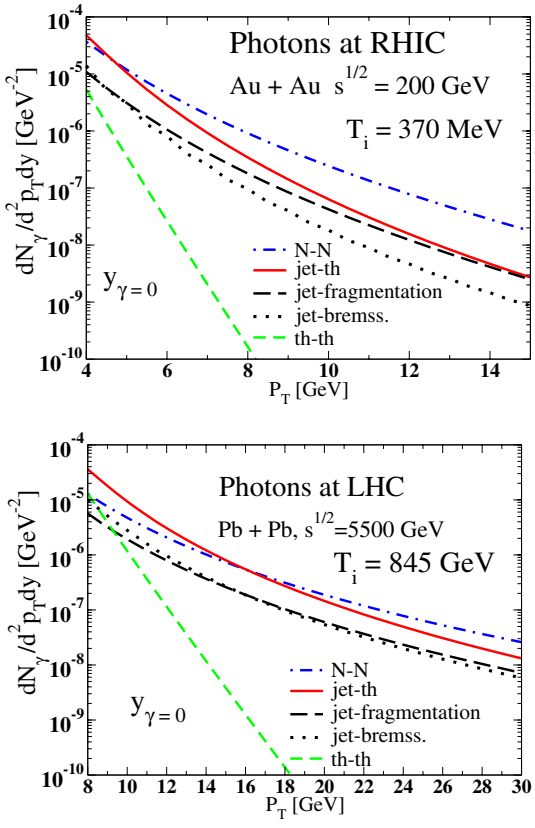

Fig. 11. Sources of high $p_{\rm T}$, mid-rapidity photons in central Au–Au collisions at RHIC (top panel), and at the LHC (lower panel). The different sources are discussed in the text

density and continued to the time-like sector and to the light cone, respectively, and convolved with the same dynamical model. It is fair to say that the SPS data do not demand a quark–gluon plasma contribution, in a direct manner. This statement also holds true for the intermediate-mass dileptons, where the radiation from thermal meson channels was also found to be quantitatively important. At RHIC and LHC energies, a complete leading-order treatment of jet energy loss in the QCD plasma has been used to calculate both pion and photon spectra. The results have been confronted with RHIC data and turn out to be in good agreement. This lends further support to the idea that high $p_{\rm T}$ suppression, for the set of kinematical conditions considered here, is a final-state effect mostly driven by gluon bremsstrahlung in the hot medium.

Acknowledgements. It is a pleasure to thank my collaborators on much of the work presented here: Sangyong Jeon, Ioulia Kvasnikova, Guy D. Moore, Ralf Rapp, Dinesh K. Srivastava, and Simon Turbide. I also thank Simon Turbide for a critical reading of this paper. This work was supported in part by the Natural Sciences and Engineering Research Council of Canada, and in part by the Fonds Nature et Technologies of Quebec. I am grateful to the Service de Physique Théorique, CEA/Saclay, for providing facilities and support used in the completion of this work.

References

1. M.A. Mazzoni et al., Nucl. Phys. A **566**, 95c (1994); M. Masera et al., Nucl. Phys. A **590**, 93c (1995)
2. See, for example, J.P. Wessels et al., Nucl. Phys. A **715**, 262c (2003), and references therein
3. See, for example, R. Rapp, J. Wambach, Adv. Nucl. Phys. **25**, 1 (2000)
4. Charles Gale, Kevin L. Haglin, Quark–gluon plasma 3, edited by R. Hwa, X.-N. Wang (World Scientific, Singapore 2004)
5. W. Cassing, E.L. Bratkovskaya, Phys. Rep. **308**, 65 (1999)
6. G.E. Brown, Mannque Rho, Phys. Rep. **363**, 85 (2002)
7. H.A. Weldon, Phys. Rev. D **42**, 2384 (1990); Charles Gale, Joseph I. Kapusta, Nucl. Phys. B **357**, 65 (1991)
8. J.J. Sakurai, Currents and mesons (University of Chicago Press, Chicago 1969); H.B. O'Connel, B.C. Pearse, A.W. Thomas, A.G. Williams, Prog. Part. Nucl. Phys. **39**, 201 (1997)
9. Ralf Rapp, Charles Gale, Phys. Rev. C **60**, 024903 (1999)
10. S. Jeon, P.J. Ellis, Phys. Rev. D **58**, 045013 (1998); V.L. Eletsky, B. Ioffe, J.I. Kapusta, Eur. Phys. J. A **3**, 381 (1998)
11. V.L. Eletsky, M. Belkacem, P.J. Ellis, Joseph I. Kapusta, Phys. Rev. C **64**, 035202 (2001)
12. P. Huovinen, M. Belkacem, P.J. Ellis, Joseph I. Kapusta, Phys. Rev. C **66**, 014903 (2002)
13. Charles Gale, Peter Lichard, Phys. Rev. D **49**, 3338 (1994)
14. E.V. Shuryak, Phys. Lett. B **78**, 150 (1978)
15. K. Kajantie, J. Kapusta, L. McLerran, A. Mekjian, Phys. Rev. D **34**, 2746 (1986)
16. Song Gao, Charles Gale, Phys. Rev. C **57**, 254 (1998)
17. See, for example, S.I. Dolinsky et al., Phys. Rep. **202**, 99 (1991), and references therein
18. Z. Huang, Phys. Lett. B **361**, 131 (1995), and private communication
19. N. Albrecht et al., Phys. Lett. B **185**, 223 (1987)
20. Ioulia Kvasnikova, Charles Gale, Dinesh Kumar Srivastava, Phys. Rev. C **65**, 064903 (2002)
21. M. Masera et al., Nucl. Phys. A **590**, 93c (1995); A.L.S. Angelis et al., Eur. Phys. J. C **13**, 433 (2000)
22. M.C. Abreu et al., Eur. Phys. J. C **14**, 443 (2000)

23. O. Drapier, private communication
24. A. Shor, Phys. Lett. B **233**, 231 (1989); B **252**, 722 (1989)
25. Z. Lin, X.-N. Wang, Phys. Lett. B **444**, 245 (1998)
26. G.Q. Li, C. Gale, Phys. Rev. Lett. **81**, 1572 (1998); Phys. Rev. C **58**, 2914 (1998)
27. Ralf Rapp, Edward Shuryak, Phys. Lett. B **473**, 13 (2000)
28. K. Gallmeister, B. Kämpfer, O.P. Pavlenko, Phys. Lett. B **473**, 20 (2000)
29. G. Usai, Eur. Phys. J. C **43**, (2005)
30. M.M. Aggarwal et al., Phys. Rev. Lett. **85**, 3595 (2000)
31. A. Dumitru, Phys. Rev. C **51**, 2166 (1995); D.K. Srivastava, B. Sinha, Phys. Rev. C **64** 034902 (2001); P. Huovinen, P.V. Ruuskanen, S.S. Räsänen, Phys. Lett. B **535**, 109 (2002)
32. M.-A. Halasz, J.V. Steele, G.Q. Li, G.E. Brown, Phys. Rev. C **58**, 365 (1998); D.K. Srivastava, K. Geiger, Phys. Rev. C **58**, 1734 (1998); P. Huovinen, M. Belkacem, P.J. Ellis, J.I. Kapusta, Phys. Rev. C **66**, 014903 (2002)
33. R. Rapp, J. Wambach, nucl-th/0001014; K. Gallmeister, B. Kämpfer, O.P. Pavlenko, Phys. Rev. C **62**, 057901 (2000)
34. Simon Turbide, Ralf Rapp, Charles Gale, Phys. Rev. C **69**, 014903 (2004)
35. H. Gomm, Ö. Kaymakcalan, J. Schechter, Phys. Rev. D **30**, 2345 (1984)
36. J. Kapusta, P. Lichard, D. Seibert, Phys, Rev. D **44**, 2772 (1991); **47**, 4171E (1991)
37. Peter Arnold, Guy D. Moore, Laurence G. Yaffe, JHEP **0206**, 030 (2002); **0112**, 009 (2001); **0111**, 057 (2001)
38. M. Asakawa, T. Hatsuda, Y. Nakahara, Prog. Part. Nucl. Phys. **46**, 459 (2001); F. Karsch, E. Laermann, P. Petreczky, S. Stickan, I. Wetzorke, Phys. Lett. B **530**, 147 (2002)
39. P. Braun-Munzinger, I. Heppe, J. Stachel, Phys. Lett. B **465**, 15 (1999); P. Braun-Munzinger, D. Magestro, J. Stachel, K. Redlich, Phys. Lett. B **518**, 41 (2001)
40. P. Aurenche et al., Eur. Phys. J. C **9**, 107 (1999)
41. D.K. Srivastava, Eur. Phys. J. C **22**, 129 (2001)
42. R. Ralf, J. Wambach, Eur. Phys. J. A **6**, 415 (1999)
43. C. Adler et al., Phys. Rev. Lett. **90**, 082302 (2003)
44. Carl Gagliardi, Eur. Phys. J. C **43**, (2005); Brian Cole, Eur. Phys. J. C **43**, (2005); Gunther Roland, Eur. Phys. J. C **43**, (2005); Jens Jorgen Gaardhoje, Eur. Phys. J. C **43**, (2005)
45. S.S. Adler et al., Phys. Rev. Lett. **91**, 072301 (2003); J. Adams et al., Phys. Rev. Lett. **91**, 172302 (2003)
46. R. Baier, Y.L. Dokshitzer, A.H. Mueller, S. Peigné, D. Schiff, Nucl. Phys. B **484**, 291 (1997); R. Baier, Y.L. Dokshitzer, A.H. Mueller, D. Schiff, JHEP **0109**, 033 (2001)
47. Enke Wang, Xin-Nian Wang, Phys. Rev. Lett. **89**, 162301 (2002)
48. Ivan Vitev, Miklos Gyulassy, Phys. Rev. Lett. **89**, 252301 (2002)
49. Alexander Kovner, Urs Achim Wiedemann, Quark-Gluon Plasma 3, edited by R. Hwa (World Scientific, Singapore, 2003)
50. B.G. Zakharov, JETP Lett. **63**, 952 (1996); **65**, 615 (1997); **70**, 176 (1999)
51. P. Arnold, G.D. Moore, L. Yaffe, JHEP **0111**, 057 (2001); **0206**, 030 (2002)
52. Simon Turbide, Charles Gale, Sangyong Jeon, Guy D. Moore, hep-ph/0502248
53. P. Aurenche et al., Nucl. Phys. B **286**, 553 (1987); B **297**, 661 (1988)
54. K.J. Eskola, V.J. Kolhinen, C.A. Salgado, Eur. Phys. J. C **9**, 61 (1999)
55. R.J. Fries, B. Müller, D.K. Srivastava, Phys. Rev. Lett. **90**, 132301 (2003)
56. R. Baier, H. Nakkagawa, A. Niegawa, K. Redlich, Z. Phys. C **53**, 433 (1992)
57. J. Frantz et al., J. Phys. G **30**, s1003 (2004)